## Title

Recovery of consolidation after sleep following stroke—interaction of slow waves, spindles, and GABA



## Journal

Cell Reports, 38(9)

## ISSN

2639-1856

## Authors

Kim, Jaekyung
Guo, Ling
Hishinuma, April
et al.

## Publication Date

2022-03-01

## DOI

10.1016/j.celrep.2022.110426

Peer reviewed

Published in final edited form as:

*Cell Rep*. 2022 March 01; 38(9): 110426. doi:10.1016/j.celrep.2022.110426.

# Recovery of consolidation after sleep following stroke – interaction of slow waves, spindles and GABA

**Jaekyung Kim**[1,2], **Ling Guo**[1,2], **April Hishinuma**[1,2], **Stefan Lemke**[1,2], **Dhakshin S. Ramanathan**[1,2,#], **Seok-Joon Won**[1,2,*], **Karunesh Ganguly**[1,2,*]

[1]Neurology and Rehabilitation Service, San Francisco Veterans Affairs Medical Center, San Francisco, California, USA.

[2]Department of Neurology, University of California-San Francisco, San Francisco, California, USA.

## Graphical Abstract

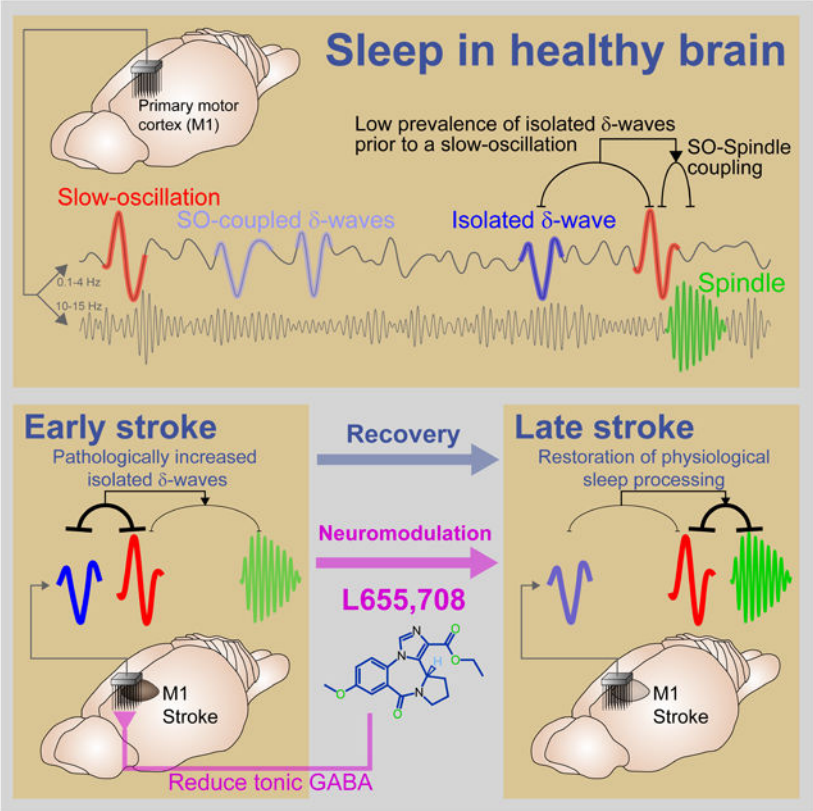


[*]Karunesh Ganguly, MD PhD, 1700 Owens Street, San Francisco, CA, 94158, USA, karunesh.ganguly@ucsf.edu; Seok-Joon Won, PhD, 1700 Owens Street, San Francisco, CA, 94158, USA, seokjoon.won@va.gov.

[#]Current Address: Mental Health Service, VA San Diego Health System, San Diego, San Diego, CA, USA. Department of Psychiatry, University of California, San Diego, San Diego, CA, USA.

**Author Contributions.** JK, LG, DSR, SW and KG conceived and designed the experiments. JK, LG, AH, SL, and SW conducted the experiments. JK analyzed all data, LG analyzed the data for Figure 1B, and AH analyzed the data for Figures 2D and E. JK and KG wrote and edited the manuscript.

**Declaration of Interests.** The authors declare no competing interests.

**Keywords**

sleep; experimental focal stroke; spindles; slow-oscillations; delta-waves; motor recovery

Sleep is known to promote recovery after stroke. Yet, it remains unclear how stroke affects neural processing during sleep. Using an experimental stroke model in rats along with electrophysiological monitoring of neural firing and sleep microarchitecture, here we show that sleep processing is altered by stroke. We found that the precise coupling of spindles to global slow-oscillations (SO), a phenomenon that is known to be important for memory consolidation, appeared to be disrupted by a pathological increase in "isolated" local delta waves. The transition from this pathological to a physiological state – with increased spindle coupling to SO – was associated with sustained performance gains during recovery. Interestingly, post-injury sleep could be pushed towards a physiological state via a pharmacological reduction of tonic GABA. Together, our results suggest that sleep processing after stroke is impaired due to an increase in delta waves and that its restoration can be important for recovery.

## INTRODUCTION

Stroke is a leading cause of motor disability; despite advancements in rehabilitation, there are no widely used therapies to augment plasticity and improve function (Ganguly et al., 2013; Macdonell et al., 1988; Norrving and Kissela, 2013). Importantly, it is now clear that a major function of sleep is to regulate neuroplasticity (de Vivo et al., 2017; Genzel et al., 2014; Gulati et al., 2017; Gulati et al., 2015; Helfrich et al., 2018; Kim et al., 2019; Klinzing et al., 2019; Latchoumane et al., 2017; Ramanathan et al., 2015; Stickgold, 2005; Tononi and Cirelli, 2014; Yang et al., 2014). Thus, optimizing sleep processing during rehabilitation has the great potential to enhance recovery. While both clinical and preclinical studies of stroke have demonstrated that sleep can influence motor recovery after stroke (Backhaus et al., 2018; Baumann et al., 2006; Duss et al., 2017; Facchin et al., 2020; Gao et al., 2010; Giubilei et al., 1992; Gottselig et al., 2002; Poryazova et al., 2015; Siengsukon and Boyd, 2009), it remains unclear precisely how sleep processing is affected by stroke.

In general, sleep-dependent processing has been closely linked to memory consolidation or the process of transforming newly encoded information into more stable long-term memories (Born et al., 2006; Stickgold, 2005). While consolidation is most studied for hippocampal-cortical interactions (Ito et al., 2015; Molle et al., 2006; Rothschild et al., 2017; Sirota et al., 2003), sleep is also known to benefit motor memories (Kim et al., 2019; Korman et al., 2007; Lemke et al., 2021; Walker et al., 2002). Specifically, NREM sleep is associated with reactivation of neural ensembles linked to movement control and performance gains after sleep (termed 'offline' gains) (Gulati et al., 2017; Kim et al., 2019; Ramanathan et al., 2015). Notably, memory consolidation is known to require the precise coupling of sleep spindles to global slow-waves, i.e., slow-oscillations (SO) (Born et al., 2006; Buzsáki, 2015; Cairney et al., 2018; Helfrich et al., 2018; Kim et al., 2019; Latchoumane et al., 2017; Maingret et al., 2016; Ngo et al., 2013). Thus, a key goal of this study was to characterize how sleep oscillations are affected by an experimentally induced

focal cortical stroke and how their characteristics may influence recovery of sleep-associated gains in task performance, i.e., consolidation.

What might be the features of sleep that are altered by an experimentally induced stroke? Recent work has shown that the balance between global SO and local slow-waves – delta-waves (δ) – determines whether there is an enhancement of skill or, instead, forgetting (Kim et al., 2019). Intriguingly, recordings in stroke patients (Poryazova et al., 2015; Sarasso et al., 2020; Tu-Chan et al., 2017; van Dellen et al., 2013) and in animal models of stroke (Burns, 1951; Burns and Webb, 1979; Carmichael and Chesselet, 2002; Gulati et al., 2015; Nita et al., 2007) have found a prevalence of *local* low-frequency power (< 4 Hz) during awake periods; this also appears to be far more common after a cortical than a subcortical lesion (Macdonell et al., 1988). Intriguingly, δ-waves may also be apparent in sleep periods after stroke (Poryazova et al., 2015). Together, these observations suggest the possibility that the sleep microarchitecture after a cortical stroke might contain more δ-waves relative to SO, thereby impairing sleep-associated “strengthening” of memory, i.e., bias sleep processing towards a “forget” state.

Here, we demonstrate that after induction of an experimental cortical stroke, the sleep microarchitecture of the perilesional cortex (PLC) is altered such that there is a reduced coupling of sleep spindles to SO. With the recovery of motor function, there was a redistribution of sleep spindles towards a more physiological state, characterized by an increase in precise spindle-SO coupling and stronger post-training offline gains after sleep. We also found that there was a concomitant reduction in local δ-waves. Interestingly, there was a direct correlation between the rate of local δ-waves and the precise coupling of spindles to SO. Remarkably, the post-stroke$_{exp}$ imbalance between δ-waves and SO could be modulated by a pharmacological treatment that reduced $GABA_A$-mediated tonic inhibition (Clarkson et al., 2010). Together, our results suggest that restoration of sleep processing may allow animals to build upon daily training and allow sustained offline performance gains.

## RESULTS

### Changes in spindle-SO nesting over recovery

We used a focal cortical stroke model (stroke$_{exp}$) (Clarkson et al., 2010; Ramanathan et al., 2018; Roome et al., 2014) to examine alterations in NREM sleep microarchitecture during recovery (Figure 1A); we implanted microelectrode arrays in the premotor cortex (i.e., perilesional cortex or PLC, n = 8, Table S1). We measured retrieval success in a single pellet task (Figures 1B and S1A); this reach-to-grasp task is a sensitive measure of prehension (Guo et al., 2021; Ramanathan et al., 2018; Whishaw et al., 1986; Wong et al., 2015). The first monitored session was 1-2 weeks after stroke$_{exp}$ (STAR Methods). Each animal experienced task training for 6-11 sessions over a period of 2-3 weeks (performance in Figure S1B). Given the variability of recovery, each animal’s sessions were divided into tertiles, ‘early’, ‘middle’, and ‘late’. We first focused on the “pre-training” sleep (sleep immediately prior to training); SO, δ-waves and spindles were identified using the filtered local field potential (LFP) (Figure 1C, STAR Methods). Sleep was detected using video analysis and NREM sleep was detected using power spectral density (Figure S2; STAR Methods) (Kim et al., 2019). We examined changes in temporal interactions of spindles to

SO within the pre-training sleep. The pre-training sleep likely reflects general changes in sleep microarchitecture and is unlikely to reflect the immediate consequence of task training.

In the healthy brain, nesting of spindles to SO is known to be essential for consolidation, (Antony et al., 2018; Bergmann and Born, 2018; Cairney et al., 2018; Helfrich et al., 2018; Kim et al., 2019; Latchoumane et al., 2017; Maingret et al., 2016; Ngo et al., 2013; Staresina et al., 2015). It also is important for triggering offline gains (Kim et al., 2019; Lemke et al., 2021; Ramanathan et al., 2015; Silversmith et al., 2020). We thus focused on comparing the "nesting" of spindles to SO in the PLC (Figure 1D; STAR Methods). More specifically, we measured temporal lags between a SO and its nearest spindle ($\Delta T_{SO\text{-}Spindle}$). With recovery, SO-Nesting became more probable (Figure 1E) and the distribution of $\Delta T_{SO\text{-}Spindle}$ became sharper, indicating spindles were occurring closer to SO (Figure 1F). Furthermore, from the distribution of $\Delta T_{SO\text{-}Spindle}$, the SO-Nesting was quantified by the probability of spindles within the nesting window (Figure 1F gray box,−0.5-1s from SO up-states). SO-Nesting significantly increased over the period of motor recovery (Figure 1G). Moreover, there was a strong increase in SO-Nesting in the late compared to the early period (Figure 1H). We also examined the rates of SO-nested spindles and found a significant increase in the late compared to the early period (early, n = 16 sessions in 8 rats, 10.1 ± 0.60 count/min vs. late, n = 16 sessions in 8 rats, 12.3 ± 0.63 count/min, LME, $t_{30} = 2.52$, P = 0.017; Figure S3). Notably, there was a significant positive relationship between the restoration of SO-Nesting and improvements in task performance (Figure 1B vs. Figure 1G; LME fit, R = 0.38, P = 0.031). Interestingly, SO-nested spindles were also associated with a significantly stronger spike modulation-depth/MD and amplitudes at the late versus the early period (MD, Figure 1I; amplitude: LME, $t_{30} = 2.26$, P = 0.031, Figure S4). Taken together, these results indicate a change in the precise temporal coupling of spindles and SO during recovery.

## Changes in sleep microarchitecture after task training.

We wondered how task training affected the sleep microarchitecture. Past work has shown that task training in the healthy brain can induce short-term changes in spindle-SO coupling, i.e., short-term "reactive" effects after training (Figure 2A). Interestingly, we found that sessions in the "late" period demonstrated greater increases in spindle-SO nesting following training compared to the "early" period (Figure 2B). The rate of SO-nested spindles did not change (early vs. late, LME, $t_{30} = 1.27$, P = 0.21; Figure S5). When we examined within-session changes in task performance (Figures 1A and 2A), we found a significant trend in the correlation between changes in SO-nesting and offline gains (LME fit, R = 0.28, P = 0.049). Interestingly, changes in SO-Nesting were more clearly linked to changes in task performance the following day (LME fit, R = 0.80, P = 0.045; Figure 2C). In other words, with continued recovery time after $stroke_{exp}$, motor training appeared to be able to trigger reactive changes in the subsequent sleep period; this appeared to manifest as improved performance the following day. This is consistent with findings that a full night of sleep results in changes in functional connectivity (Lemke et al., 2021).

Is it also possible that there is a direct relationship between sleep duration and offline gains? We performed experiments in separate groups with $stroke_{exp}$ to test this (Figures 2D and E). We specifically assessed the effects of sleep duration on offline gains during *middle-late*

*phase* of recovery, i.e., when each animal demonstrated performance improvements. In other words, we did not use *early* period linked to abnormal sleep activity. In this separate group, we measured the effects of sleep on the task and compared these to a sleep restriction group (Figure 2D). For the sleep group (sleep: n = 29 sessions in 6 rats), we measured sleep duration using video-based detection. In the restriction group (no-sleep: n = 28 sessions in 8 rats), sleep was restricted either 2-6 hours after training and then the retrieval was conducted. The rats with post-training sleep experienced greater offline gains in task performance in comparison to the sleep-restricted animals (sleep: 6.4 ± 1.8% vs. no-sleep: −2.5 ± 2.3%, two-sample *t*-test, $t_{55} = 2.28$, P = 0.027). We also found a significant relationship between sleep duration and task performance in he middle-late period (LME fit, R = 0.52, P = 0.022; Figure 2E); however, there was no significant relationship when including the early phases of recovery (LME fit, R = 0.25, P = 0.25). We interpreted these results to mean that sleep-associated processing might be beneficial after an initial early phase". Together, these results suggest a precise dose-outcome relationship between sleep duration and gains.

## Pathological local δ-waves

We next examined changes in the temporal interactions of δ-waves with SO and spindles. For the pre-training sleep shown in Figure 1, δ-waves were also identified using the filtered LFP at 0.1-4 Hz (Figure 3A; STAR Methods). We then measured the temporal relationship between δ-waves and SO ($\Delta T_{SO\text{-}\delta}$) in two groups of rats (photothrombotic/PT $stroke_{exp}$ in M1, n = 8 rats and healthy rats, n = 5; Figure 3B). In healthy animals, δ-waves typically follow SO. We then compared it to the early period after $stroke_{exp}$. Interestingly, in the early period, there was a significant increase in δ-waves that were apparently decoupled from SO, i.e., temporally far from the previous SO. All $stroke_{exp}$ animals demonstrated this effect compared to healthy animals (Figure 3C; Figure S6). Using the $50^{th}$ percentile of this distribution, we separated δ-waves into two classes, "SO-coupled/$\delta_{SO}$" and "isolated/$\delta_I$" (STAR Methods). Notably, the overall ratios of SO/δ were similar in both $stroke_{exp}$ and healthy animals ($stroke_{exp}$: 27.9 ± 2.2% vs. healthy: 32.4 ± 2.6%, two-sample *t*-test, $t_{23} = -1.31$, P = 0.24). Thus, after $stroke_{exp}$, while the relative number of SO and δ-waves were comparable to the healthy state, there was a significant increase in the prevalence of $\delta_I$-waves not temporally coupled to a SO. We also examined changes in the temporal interactions of spindles to $\delta_I$-waves in the PLC. We analyzed "$\delta_I$-Nesting" in a similar manner to "SO-Nesting," i.e., its closest spindle (Figure 3D; STAR Methods). With recovery, $\delta_I$-Nesting significantly decreased over recovery (Figure 3E). Moreover, there was a moderate decrease in the late compared to the early period (Figure 3F). We also examined the rates of $\delta_I$-nested spindles and found no significant change (early, n = 16 sessions in 8 rats, 10.3 ± 0.70 count/min vs. late, n = 16 sessions in 8 rats, 11.1 ± 0.51 count/min, LME, $t_{30} = 1.18$, P = 0.25; Figure S3). Notably, there was a negative relationship between the decrease of $\delta_I$-Nesting and time-dependent improvements in task performance (Figure 1B vs. Figure 3E; LME fit, R = –0.43, $P < 10^{-2}$). The relative nesting, i.e., SO-Nesting/$\delta_I$-Nesting was more predictive of recovery compared to SO-Nesting (SO-Nesting/$\delta_I$-Nesting: LME fit, R = 0.46, $P < 10^{-2}$; smaller absolute errors between true and predicted performances by SO-Nesting/$\delta_I$-Nesting versus SO-Nesting: paired *t*-test, $t_{31} = 2.18$, P = 0.037). Together, these results indicate there was a change in the precise temporal coupling of spindles toward SO and away from $\delta_I$-waves with recovery.

### Relationship between local $\delta_I$-waves preceding SO and nesting

Is there a more direct relationship of these observed changes in $\delta_I$-waves on SO-spindle nesting? Past studies have shown that changes in SO parameters (e.g., amplitude) can depend on the temporal proximity of slow-waves (Bernardi et al., 2018; Ngo et al., 2015). Given the changes we observed in SO-Nesting with recovery, we examined whether changes in how often $\delta_I$-waves directly preceded a SO event could predict this. We examined how many $\delta_I$-waves preceded SO, i.e., −5-0s from SO up-state (Figure 3G). Remarkably, this appeared to significantly influence spindle nesting to SO; we found a strong negative correlation between the $\delta_I$-wave rate preceding SO and SO-Nesting (Figure 3H). Furthermore, the rate of $\delta_I$-waves preceding SO had a significant negative correlation with the task-performance the following day (Figure 3I) as well as the within-session changes in task performance (LME fit, R = 0.30, P = 0.032). Thus, our results suggest that the prevalence of $\delta_I$-waves in the early phase can influence the nesting of spindles to SO and changes in performance.

### Reducing elevated tonic inhibition and pathological sleep

What might be the underlying neurophysiological basis for our observed changes in SO and $\delta_I$-waves with recovery? One possibility is that elevations in extra-synaptic γ-aminobutyric acid (GABA) after $\text{stroke}_{exp}$ may alter local excitability and thus perturb the ability of global SO to organize local δ. Studies have reported that reducing such tonic inhibition can have a beneficial effect on recovery (Clarkson et al., 2010; He et al., 2019); implying that altered excitation-inhibition/E-I balance (Kim and Fiorillo, 2017; Xia et al., 2017; Yizhar et al., 2011) plays a role in recovery.

We tested the effects of blocking $\text{GABA}_A$ tonic inhibition after $\text{stroke}_{exp}$ on the coupling of spindles to slow-waves. For these experiments, we only tested this intervention during the early spontaneous recovery period; this allows us to examine changes in the absence of contributions from task training. We injected the $\text{GABA}_A$ α5-subtype receptor inverse agonist (L655-708) (Clarkson et al., 2010) during early recovery after a PT $\text{stroke}_{exp}$ (n = 3 rats) or Endothelin-1 (ET-1) $\text{stroke}_{exp}$ (n = 3 rats). The ET-1 approach allowed us to collect baseline neural data prior to stroke induction (STAR Methods). This was followed by recordings after the injection of vehicle (sham) or L655-708 (drug) during early recovery, i.e., days 7~12 after $\text{stroke}_{exp}$ (Figure 4A).

Strikingly, treatment with the drug resulted in significantly stronger SO-spindle nesting with a concomitant reduction in $\delta_I$-spindle nesting (Figure 4B). Notably, drug infusion in a separate group of healthy animals resulted in stronger $\delta_I$-spindle nesting with non-significant changes in SO-spindle nesting (Figure S7; SO-Nesting: sham, n = 9 sessions in 3 rats, 28.4 ± 0.73% vs. drug, n = 9 sessions in 3 rats, 26.8 ± 1.7%, LME, $t_{16} = -1.14$, P = 0.27; $\delta_I$-Nesting: sham, 35.2 ± 1.1% vs. drug, 38.7 ± 1.3%, LME, $t_{16} = 3.59$, $P < 10^{-2}$). This suggests that the beneficial effect of the drug is specific for $\text{stroke}_{exp}$ and perhaps detrimental in healthy animals (see Discussion). In $\text{stroke}_{exp}$ animals, we also observed increased excitability; the unit MD during SO was stronger (Figure 4C). Moreover, changes in the unit MD during spindles, a measure of the effectiveness of spindles in modulating local spiking, could be explained by an increase in SO-nesting (Figure 4D). We did not

find any differences i for the ET-1 and PT groups (ET-1 vs. PT; ΔSO-Nesting: two-sample *t*-test, $t_{15} = -0.14$, P = 0.89; ΔSpindles-MD: two-sample *t*-test, $t_{15} = -0.064$, P = 0.95). Notably, for SO-spindle nesting and $\delta_I$-spindle nesting, sham showed significant differences compared to the baseline, i.e., drop in SO-spindle nesting and increase in $\delta_I$-spindle nesting after $stroke_{exp}$, while the drug was not significantly different from the baseline (SO-Nesting: sham vs. baseline, LME, $t_{13} = 3.93$, P = 1.7 x $10^{-3}$, drug vs. baseline, LME, $t_{13} = 2.01$, P = 0.067; $\delta_I$-Nesting: sham vs. baseline, LME, $t_{13} = -3.09$, P = 8.6 x $10^{-3}$, drug vs. baseline, LME, $t_{13} = -1.55$, P = 0.15). Thus, our results indicate that elevated $GABA_A$-mediated tonic inhibition can alter the sleep microarchitecture.

## DISCUSSION

Our results suggest a roadmap to delineate normal vs pathological sleep after stroke; they also suggest novel therapeutic targets to modulate sleep processing (e.g., tonic GABA and SO-spindle nesting) in order to enhance recovery (Figure S8).

### Sleep and memory consolidation post-stroke

EEG studies in patients (Macdonell et al., 1988; Poryazova et al., 2015; Tu-Chan et al., 2017; van Dellen et al., 2013) and LFP recordings in animal models (Carmichael and Chesselet, 2002; Gulati et al., 2015) have found increased low-frequency power during awake periods. These studies have indicated that this increased low-frequency power is a marker of cortical injury and loss of subcortical inputs (Topolnik et al., 2003). Our findings of increased local $\delta_I$-waves are perhaps related to this phenomenon. Importantly, the increased frequency of $\delta_I$-waves preceding SO was closely associated with the attenuated coupling of spindles to SO (Figure 3H). We further found evidence for normalization of SO-$\delta_I$ interactions with recovery and task training.

In general, there is growing evidence that the temporal coupling of spindles to SO are essential drivers of memory consolidation during sleep (Antony et al., 2018; Cairney et al., 2018; Helfrich et al., 2018; Kim et al., 2019; Latchoumane et al., 2017; Maingret et al., 2016; Staresina et al., 2015). Such coupling has been linked to spike-time dependent plasticity (Bergmann and Born, 2018). It is also a potent driver of the reactivation of awake experiences (Antony et al., 2018; Cairney et al., 2018; Ngo et al., 2013; Peyrache et al., 2009). Finally, disruption of this coupling has been found to impair memory consolidation after awake experiences (Kim et al., 2019). Thus, our results suggest a link between pathological changes in network physiology after $stroke_{exp}$ to impaired sleep-associated processing, primarily via disruption of precise spindle-SO coupling.

It is important to note that our observations of changes in sleep microstructure during recovery are largely correlational at this stage. It is difficult for us to distinguish the effect of a deficient capacity of encoding during awake training from our observed changes in sleep processing and offline gains following sleep. For example, it is likely that with recovery, more effective task performance and associated ensemble dynamics (Guo et al., 2021; Khanna et al., 2021; Ramanathan et al., 2018) also influence the efficacy of sleep processing. However, it is worth pointing out that precise manipulations of sleep processing in healthy animals are sufficient to prevent offline gains even when awake task learning

was robust. For example, our recent study found that relatively precise modulation of the extent of sleep spindle-SO coupling in healthy animals could either enhance or impede sleep processing (Kim et al., 2019). Future studies using such precise modulation approaches can causally test whether manipulation of sleep processing after $stroke_{exp}$ is sufficient to enhance or impede motor recovery.

### Implications for rehabilitation

We found that changes in sleep processing after $stroke_{exp}$ were correlated with offline gains during recovery. Importantly, clinical rehabilitation approaches are quite varied and not simply equal to task training; moreover, there are differences in training that aim to restore function as opposed to enabling compensation (Bernhardt et al., 2017; Ganguly et al., 2013; Pearson-Fuhrhop et al., 2009). Even so, our reach training offers a way to study functional recovery in both rodents and non-human primates (Guo et al., 2021; Khanna et al., 2021; Ramanathan et al., 2018; Whishaw et al., 1986). Based on this, our results specifically suggest that marking whether sleep is pathological or physiological may be an important consideration for timing rehabilitation. Interestingly, past studies in humans and rodents have suggested a sensitive period in which training can trigger long-term benefits (Dromerick et al., 2021; Dromerick et al., 2009; Krakauer et al., 2012). Notably, if it is indeed the case that awake low-frequency power in stroke patients is related to our observed effects on sleep processing, it might help explain past results indicating that awake low-frequency power is a predictor of recovery. EEG studies can also delineate when and if the transition to physiological sleep occurs and whether this is related to the sensitive period.

### Implications for therapeutic neuromodulation

Our results have implications for translational studies. Animal studies have suggested that $GABA_A$-mediated tonic inhibition in the PLC may be a therapeutic target to promote recovery; blockade of $GABA_A$-mediated tonic inhibition was found to promote motor recovery maximally within the first 1~2 weeks in mice (Clarkson et al., 2010; He et al., 2019). Both short-term (i.e., acutely prior to training) and long-term chronic infusion have been tested. Intriguingly, long-term infusion appears to be better (Clarkson et al., 2010). Although our pharmacological experiments were performed in a separate group of animals without motor training, our results provide a possible mechanism for why long-term infusion by Clarkson and colleagues may be essential to achieve prominent benefits; more specifically, the effect of this drug might not only help with task-specific online training, i.e., encoding motor skills during awake training, but also promote offline memory consolidation during sleep. Future work can better define the causal role of drug manipulation during sleep in the recovery of motor function after stroke.

Our results also suggest possible approaches to neuromodulation to enhance recovery. It is quite likely that SO and δ-waves can be monitored using EEG recordings in stroke patients. Moreover, non-invasive brain stimulation during sleep (Antony et al., 2018; Cairney et al., 2018; Marshall et al., 2006; Ngo et al., 2013) can be tailored based on suppressing δ-waves waves or enhancing SO. It is also possible that invasive approaches for neuromodulation after stroke (Levy et al., 2016) can also focus on optimizing sleep processing. For example, while recent studies have shown that direct electrical stimulation can enhance awake

performance after $stroke_{exp}$ (Khanna et al., 2021; Ramanathan et al., 2018), there has been less of a focus on extending this to sleep periods. Interestingly, a recent study suggested that neuromodulation to modulate up-states during sleep can enhance recovery (Facchin et al., 2020). It is quite possible that closed-loop neuromodulation approaches that focus on both optimizing task performance and its consequence during sleep processing (Kim et al., 2019) may lead to the greatest long-term benefits during rehabilitation.

## STAR★METHODS

### RESOURCE AVAILABILITY

**Lead contact—**Further information and requests for resources and reagents should be directed to and will be fulfilled by the Lead Contact, Karunesh Ganguly (karunesh.ganguly@ucsf.edu).

**Materials availability—**This study did not generate new unique reagents.

**Data and code availability—**The datasets supporting the current study have not been deposited in a public repository because they are still being used for current studies, but are available from the Lead Contact upon reasonable request.

Custom MATLAB code for the detection of SO, δ-waves, and spindles will be shared by the Lead Contact upon reasonable request.

Any additional information required to reanalyze the data reported in this work paper is available from the Lead Contact upon reasonable request.

### EXPERIMENTAL MODEL AND SUBJECT DETAILS

Experiments were approved by the Institutional Animal Care and Use Committee at the San Francisco VA Medical Center. We used a total of twenty eight adult Long-Evans male rats (250–400 g; Charles River Laboratories); twenty six rats with focal experimental stroke ($stroke_{exp}$) and two rats without $stroke_{exp}$ (Table S1; detailed contributions of each rat on the respective results). No statistical methods were used to predetermine sample sizes, but our sample sizes are similar to those reported in previous publications (Gulati et al., 2017; Gulati et al., 2014; Guo et al., 2021; Kim et al., 2019). Animals were kept under controlled temperature and a cycle with 12-h light and 12-h dark (lights on at 06:00 a.m.). Animals were pair-housed prior to electrode/cannula implantation and then singly housed after to prevent damage to implants. If applicable, animals were randomly assigned to experimental groups.

### METHOD DETAILS

**Animals/surgery—**Surgeries were performed under isofluorane (1-3%) anesthesia and body temperature was maintained at 37 °C with a heating pad. Atropine sulfate was also administered intraperitoneal/IP before anesthesia (0.02 mg/kg of body weight). We implanted 32/128-channel microwire arrays for recording LFP/spike activity; arrays were lowered down to 1,400-1,800 μm in layer 5 of the primary motor cortex (M1) or perilesional cortex (PLC) in the upper limb area. In the healthy animals (n = 2), neural probes were

centered over the forelimb area of M1, at 3 mm lateral and 0.5 mm anterior from the bregma. In the stroke$_{exp}$ animals (n = 14), the neural probe was placed immediately anterior to the lesion site, typically centered ~3-4 mm anterior and 2.5-3 mm lateral to the bregma. The reference wire was wrapped around a screw inserted in the midline over the cerebellum. The final localization of depth was based on the quality of recordings across the array at the time of implantation. The post-operative recovery regimen included administration of buprenorphine at 0.02 mg/kg and meloxicam at 0.2 mg/kg. Dexamethasone at 0.5 mg/kg and trimethoprim sulfadiazine at 15 mg/kg were also administered postoperatively for 5 days. All animals were allowed to recover for at least five days with the same regimen as described above before the start of experiments. Data collection and analysis were not performed blind to the conditions of the experiments.

**Photothrombotic and endothelin-1 induced focal stroke$_{exp}$—**We used either photothrombotic (PT) and Endothelin-1 (ET-1) induced stroke$_{exp}$ models (see stroke$_{exp}$ types for each group of animals in Table S1). For the PT stroke$_{exp}$ model, rose bengal dye was injected into a femoral vein using and an intravenous catheter after craniotomy. Next, the surface of the brain was illuminated with white light (KL-1500 LCD, Schott) using a fiber optic cable for 20 min. We used a 4-mm aperture for stroke$_{exp}$ induction (centered in the M1 area based on stereotactic coordinates; −1.5-2.5 mm anterior and 1-5 mm lateral from the bregma) and covered the remaining cortical area with a custom aluminum foil mask to prevent light penetration. After induction, a probe was implanted in the PLC immediately anterior to the lesion site (Gulati et al., 2015; Ramanathan et al., 2018). The craniotomy and implanted electrodes were covered with a layer of low toxicity silicone adhesive (WPI KWIK-SIL), then covered by dental cement. For the precise measure of baseline of LFP/spike activity before inducing stroke$_{exp}$ (pre-stroke$_{exp}$ baseline in Figure 4A), we also used ET-1 induced focal stroke$_{exp}$ model (Robinson et al., 1990; Roome et al., 2014; Sharkey et al., 1993; Virley et al., 2004) in three rats (Figure 4). To induce ET-1 stroke$_{exp}$, microarray attached with infusion cannula (guide: 26G; internal: 33G; P1 Technology) was implanted into the M1 area; single cannula in one rat and bilateral cannula with 2 mm spacing in the other two rats. The cannula was centered at 3 mm lateral and 0.5 mm anterior from the bregma to target M1 and microarray was positioned anterior to the cannula; the lesion site and recording site were targeted to correspond to the PT stroke$_{exp}$ animals. The remaining operation procedures were the same as the PT stroke$_{exp}$ animals. The ET-1 induced stroke$_{exp}$ model allowed us to induce the focal stroke$_{exp}$ following a baseline measurement; after measuring baseline spike/LFP activity for 2 days, ET-1 was injected with 1.5 ul through a single cannula in one rat, and a total 2.0 ul (two sites injections; 1.0 ul for each) through a bilateral cannula (100 nl per min) in the other two rats into deep cortical layers (1.4 mm from the surface of the brain). We then measured spike/LFP activity during the recovery period following the ET-1 stroke$_{exp}$ induction.

**Electrophysiology—**We conducted AC-coupled recordings and recorded extracellular neural activity using 32-channel microwire electrode arrays (MEAs; 33-μm-length, 250-μm-spacing, 4-rows, standard polyimide-coated tungsten microwire arrays from Tucker-Davis Technologies (TDT) for ten rats; 25-μm-length, 200-μm-spacing, 6-rows, tungsten microwire arrays from Innovative Neurophysiology Inc. for five rats) and 128-channel

custom electrode arrays (Egert D, 2018) (for one rat). All electrode arrays showed similar quality of LFP (e.g., LFP amplitude and noise level). The microwire arrays from Innovative Neurophysiology Inc. were customized so that a cannula is placed beside the recording sites of microwires. We recorded spike and LFP activity using a 128-channel RZ2 bioamp processor (TDT) and 128-channel neurodigitizer (digital PZ4 or PZ5).

Spike data was sampled at 24,414 Hz and LFP data at 1,018 Hz. ZIF-clip-based headstages (TDT) for 32-channel microwires and SPI-based headstates (RHD 128-Channel Recording Headstage, Intan Technologies) for 128-channel microwire with a unity gain and high impedance (~1 G) was used. Only clearly identifiable units with good waveforms and a high signal-to-noise ratio were used. The remaining neural data (e.g. filtered LFP) was recorded for offline analysis at 1,018 Hz. Behavior-related timestamps (that is, trial onset and trial completion) were sent to the RZ2 analog input channel using a digital board and then used to synchronize to neural data in the offline analyses. Electrophysiology was not monitored during the baseline sessions illustrated for the pre-stroke$_{exp}$ motor performance in Figure 1 and in the animal group of Figure 2D (see Table S1 for the corresponding animals).

**Behavior—**After recovery, animals were typically handled for several days before the start of experimental sessions, i.e., “motor training sessions.” Animals were acclimated to a custom plexiglass behavioral box during this period without motor training. The box was equipped with a door at one end. We examined two groups of stroke$_{exp}$ animals; with motor training in Figures 1, 2, and 3 and with spontaneous recovery in Figure 4. In the rats used for Figure 4 (testing the effect of reducing tonic $GABA_A$), animals experienced spontaneous recovery without motor training. In the other rats of Figures 1, 2, and 3, animals were trained to a plateau level of performance in a reach-to-grasp single-pellet task before neural probe implantation or PT stroke$_{exp}$ induction (baseline; pre-stroke$_{exp}$ training period in Figure 1A). In a single session of the motor training post- stroke$_{exp}$, pre-training sleep, reach training, post-training sleep, and reach retrieval blocks were monitored in sequence. We measured relative reach performance, i.e., pellet retrieval success rate in the reach-to-grasp task, using normalized metrics relative to the baseline, Figure 1B; PT stroke$_{exp}$ impaired motor performance (baseline, n = 16 sessions in 8 rats: 100 ± 1.9% vs. early, n = 16 sessions in 8 rats: 47.8 ± 6.8%; LME, $t_{30} = -7.44$, $P < 10^{-7}$). It improved over the subsequent training (late, n = 16 sessions in 8 rats: 75.4 ± 4.7%; early vs. late, LME, $t_{30} = 5.78$, $P < 10^{-5}$). However, the absolute reach performance was compared to sleep metrics for all other analyses. The reach-to-grasp task has been used as a sensitive measure of motor function; it requires reaching, grasping, and retrieving a single pellet located at a distance outside of the behavior box (Figure S1A) (Guo et al., 2021; Ramanathan et al., 2018; Whishaw et al., 1986; Wong et al., 2015). Probe implantation and stroke$_{exp}$ induction were performed contralateral to the preferred hand. Animals were allowed to rest at least for 6 days before the start of motor training or recording sessions post-stroke$_{exp}$. The stroke$_{exp}$ animal group experienced motor training until the motor performance reached a plateau level of performance (motor performance in an individual animal is shown in Figure S1), which is called motor training post-stroke$_{exp}$ during the recovery period in Figure 1A. The first reach training session for the “across-session” analyses was between the 7-14th day (9.1±2.6, mean±s.d.); this was because of the need to restart food scheduling. Each animal

was monitored for 6-11 sessions/days until a stable plateau was reached (Figure S1). Given the variability of recovery times, and as described in the results, sessions per animal were divided into tertiles and termed ‘early’, ‘middle’ and ‘late.’ During behavioral assessments, we monitored the animals and ensured that their body weights did not drop below 90% of their initial weight. We monitored electrophysiology, i.e., LFP/spike only during the pre-training sleep, reach training, post-training sleep, and retrieval period of each session, not during 24 hours of a single day. This typically totaled a period of 4-5 hours a day in the behavior box. After completing motor tasks and sleep sessions in the behavioral box, animals were placed in the home cage without electrophysiology monitoring.

For the behavioral task, we used an automated reach-box, controlled by custom MATLAB scripts and an Arduino microcontroller. This setup for the reach-to-grasp task required minimal user intervention, as described previously (Wong et al., 2015). Each trial consisted of a pellet dispensed on the pellet tray, followed by a beep indicating that the trial was beginning; this was followed by the door opening. Animals then had to reach their arm out, grasp and retrieve the pellet. A real-time “pellet detector” using an infrared detector centered over the pellet was used to determine when the pellet was moved, which indicated that the trial was over and the door was closed. All trials were captured by video, which was synced with the electrophysiology data using the Arduino digital output. The video frame rate was 30 Hz for six animals and 75 Hz for two animals. The reach performance (the number of accurate pellet retrieval/the total number of trials x 100 %) was determined manually from a recorded video. The reach performance was used not only as a measure of motor function recovery across sessions (Figure 1B) but also as a measure of “*offline gains*” that may be the result of memory consolidation from sleep (Figure 2C). As a measure of offline gain, we computed the next-day reach performance (i.e., a change in reach performance between Day X reach training and the following Day X+1 reach training; Figure 2C) and the within-session changes (i.e., reach performance changes after post-training sleep compared to before post-training sleep, Figure 2E). These measurements allowed us to quantify offline gains and motor recovery either across sessions and within a session (see also below). For the sleep restriction experiments, i.e., no-sleep group in Figure 2D, moderate vibration on the behavior box was given when rats were not active for > 40 sec, to prevent from sleeping. In this restriction group (n = 8 rats), sleep was deprived either 2 or 6 hours after the training and then the retrieval was conducted (n = 4 restricted for 2 hours; n = 4 restricted for 6 hours).

**$GABA_A$ α5-subtype receptor inverse agonist treatment—**Treatment with the $GABA_A$ α5-subtype receptor inverse agonist (L655,708; “drug” condition in Figure 4) was initiated 6 days after ET-1 $stroke_{exp}$ induction; previous studies reported that L655,708 promoted functional recovery 7 days after $stroke_{exp}$ (Clarkson et al., 2010; He et al., 2019). About 0.5~1 hour before sleep onset, rats received intraperitoneal/IP injections of vehicle (i.e., saline as the “sham”) or L655,708 (Sigma-Aldrich; 5 mg/kg, dissolved in dimethylsulphoxide/DMSO and then diluted 1:1 in 0.9% saline as the “drug” condition). Over the course of 6 days, we used either sham or drug every other day (see experiment flow in Figure 4A). To counterbalance the starting condition between sham and drug conditions in six animals, either drug or sham was administrated IP on separate days, i.e., the drug

condition was tested every other day during range of day 7-12. The starting condition was the drug at day 7 in three rats and the sham at day 7 in the other three rats. More precisely, the sham was conducted on days 7, 9, and 11 for ET-1 induced animals (n = 3), and the drug was conducted on days 7, 9, and 11 for PT induced animals (n = 3).

**Analyses across-session versus within-session—**In the $stroke_{exp}$ experiment in Figures 1, 2, and 3, animals performed the reaching task during recovery (6-11 days of training). For long-term recovery in the $stroke_{exp}$ animal group, we specifically analyzed the "pre-training sleep" and the "reach training" over a ~3 weeks recovery period. In the other experiment, to test the effect of reducing tonic $GABA_A$ in Figure 4, we focused on spontaneous changes in sleep microarchitectures without motor training over a ~2 weeks recovery period. These analyses of the changes over a long-term recovery period are termed "across-session" analyses. In each animal, the 1-2 weeks recovery period was divided into sextiles and a representative session in each sextile was used. The motor performance and the sessions used are marked in Figures S1B. In five animals, all monitored sessions were used (i.e., two sessions per period and total of six sessions were monitored). In three animals, representative sessions (two sessions per period) were selected in order to balance the number of sessions per animal, e.g., typically every other session was selected. In Figure 2, we also compared sleep metrics within a single-day session/experiment (i.e., "within-session" analyses). Sleep metrics (e.g., SO-Nesting) were measured as a pair of pre-training and post-training sleep in a single-day session, then the change from the pre-training to the post-training sleep was computed (e.g., ΔSO-Nesting). These metrics (e.g., Day X) were then compared with the offline gains in motor performance during the reach training of the following day (e.g., Day X+1) in Figure 2C. In Figures 2D and E, the within-session offline gains in motor perfromance (i.e., changes from reach training to reach retrieval within a single session) were examined.

**Identification of NREM sleep waves—**LFP activity was recorded using 32/128-channel microwire electrode arrays (see above). The LFP was analyzed after removing obvious artifacts (> 10 s.d.) and excluding bad channels. Identification of NREM epochs was performed by classification based on power spectral density of the LFP. LFP trace was segmented into non-overlapping 6-sec epochs. In each epoch, the power spectral density was computed and averaged over the slow-wave frequency band including SO and δ-waves (0.1-4 Hz, also called Delta band) and Gamma frequency bands (30-60 Hz). Then a k-means classifier was used to classify epochs into two clusters, NREM sleep and REM/awake; REM sleep and awake were not classified and NREM sleep was focused on in this study. Sleep epochs less than 30 sec were excluded from NREM sleep epochs. The identified NREM sleep durations were not different between the early period and late period of motor recovery (Figure S2B). The identified NREM sleep epochs were verified by visual assessment of the LFP activity. During the NREM period with high Delta power (0.1-4 Hz), strong down- and up-states dominates. Thus, we assessed if our detected NREM sleep epochs contain a high-amplitude and slow LFP fluctuation distinguished from a low-amplitude and high-frequency LFP during the awake period. Moreover, we assessed if there were substantial missing detections of NREM sleep epoch; assessment if a high amplitude LFP epoch was not included in the detected NREM sleep epochs excessively. These power-based

sleep detections showed a close match to the video-based detections (Kim et al., 2019; Pack et al., 2007) (Figure S2A); the number of pixels that changed intensity frame to frame in each pair of consecutive frames was computed from a recorded video (1 Hz frame rate using Microsoft LifeCam Cinema Webcam) during the sleep block; these values were then integrated over an epoch of 40 sec. If that integrated value was higher than a threshold, that epoch was identified as sleep; the threshold was chosen by comparing detection results and visual assessment of the recorded video.

In offline analysis, SO, δ-waves and spindles were detected using the algorithm used in previous studies (Gulati et al., 2017; Kim et al., 2019; Lemke et al., 2021; Silversmith et al., 2020). The LFP average across all recording channels excluding bad channels was filtered in the SO/δ band (0.1-4 Hz) through two independent filterings; the high pass Butterworth filter (2nd order, zero phase-shifted, with a cutoff at 0.1 Hz) was applied and then followed by the low pass Butterworth filter (5th order, zero phase-shifted, with a cutoff at 4 Hz). The individual order of the high-pass and low-pass filter was estimated through a conventional minimum-order design; it requred to meet maximum passband ripple of 3 dB and minimum stopband (presumed 0.02 Hz for high-pass filter and 6 Hz for low-pass filter) attenuation of 15 dB. Next, all positive-to-negative zero crossings during NREM sleep were identified, along with the previous peaks, the following troughs, and the surrounding negative-to-positive zero crossings. Then the positive threshold (the top 15 percentile of the peaks) and the negative threshold (the bottom 40 percentile of the troughs) were respectively defined for the down-states and up-states; in Figure 1C, horizental dashed lines indicate the threshold detecting SO up/down states. Each identified wave was considered a SO if the trough was lower than the negative threshold (i.e., up-state), the peak preceding that up-state was higher than the positive threshold (i.e., down-state), and the duration between the peak and the trough was between 150 ms and 500 ms (Figures 1C and 3A). On the other hand, a slow wave was considered a δ-wave if the trough was lower than the negative threshold (i.e., up-states) and that the up-state was preceded by a maximum voltage that was lower than the positive threshold within 500 ms. In this study, we separated δ-waves into two classes (SO-coupled/$\delta_{SO}$ and isolated/$\delta_I$) depending on their temporal interaction with a preceding SO, i.e., $\Delta T_{SO\text{-}\delta}$ (Figures 3B and C). This distinction was based on simply dividing the $\Delta T_{SO\text{-}\delta}$ distributions using the $50^{th}$ percentile; δ-waves less than the $50^{th}$ percentile were labeled $\delta_{SO}$, whereas the remaining δ-waves were labeled $\delta_I$. $\Delta T_{SO\text{-}\delta} > 100$ sec (1~2%) were manually removed to exclude the cases driven by the possible error in NREM sleep detections; this error was evaluated by visual inspection of slow-wave activity. From the distribution of $\Delta T_{SO\text{-}\delta}$ in healthy brains (n = 9 sessions, 5 rats), $50^{th}$ percentile of $\Delta T_{SO\text{-}\delta}$ (3.7 sec) was set as the cutoff separating δ-waves into "$\delta_{SO}$" and "$\delta_I$" waves; δ-waves within the close 50% from a preceding SO ($\Delta T_{SO\text{-}\delta} \leq 3.7$ sec) were labeled "$\delta_{SO}$," whereas δ-waves of the distal 50% from a preceding SO ($\Delta T_{SO\text{-}\delta} > 3.7$ sec) were labeled "$\delta_I$." The cutoff of $\Delta T_{SO\text{-}\delta}$ determined by the healthy conditions was also used for $stroke_{exp}$ conditions. The distribution of $\Delta T_{SO\text{-}\delta}$ was more variable across the $stroke_{exp}$ animals; it appears to be due to the variability of lesion size. Specifically in the comparison with the same animal (Figure S6), the distribution of $\Delta T_{SO\text{-}\delta}$ after $stroke_{exp}$ appeared to be abnormal compared to the healthy condition without $stroke_{exp}$. Therefore, the cutoff of $\Delta T_{SO\text{-}\delta}$ was determined by using the healthy conditions.

For spindles detection, the LFP was first z-scored in each channel and averaged across all good channels. The LFP average was filtered in spindle band (10-15 Hz) through two independent zero phase-shifted filterings (Figures 1C and 3A); the high pass Butterworth filter (6th order, zero phase-shifted, with a cutoff at 10 Hz) was applied and then followed by the low pass Butterworth filter (8th order, zero phase-shifted, with a cutoff at 15 Hz). The individual order of the high-pass and low-pass filter was estimated through a conventional minimum-order design; it requred to meet maximum passband ripple of 3 dB, and minimum stopband (presumed 7 Hz for high-pass filter and 19 Hz for low-pass filter) attenuation of 15 dB. We computed a smoothed envelope of this signal, the magnitude of the Hilbert transforms with convolving by a Gaussian window (200 ms). Next, we determined two thresholds for spindle detection based on the mean ($\mu$) and standard deviation ($\sigma$) of the spindle band LFP during NREM sleep; the upper and lower thresholds were set $\mu + 2.5 \times \sigma$ and $\mu + 1.5 \times \sigma$, respectively; in Figure 1C, horizental dashed lines indicate the threshold detecting spindle period. Epochs in which the spindle power exceeded the upper threshold for at least one sample and the spindle power exceeded the lower threshold for at least 500 ms were considered spindles. Each epoch where the spindle power exceeded the lower threshold was considered the start and stop of the spindle; the duration of each spindle was based on these values as well.

**Spindle nesting analyses—**We also analyzed the temporal coupling of spindles relative to SO or δ-waves. For the nesting of spindles to SO (SO-Nesting; Figure 1D), each spindle was linked to the closest SO. The time difference between the peak of the spindle and the up-state of the linked SO was measured for each detected spindle ($\Delta T_{SO\text{-}Spindle}$). If $\Delta T_{SO\text{-}Spindle}$ was between −0.5 sec and 1.0 sec (i.e., nesting time window), that spindle event was considered a SO-nested spindle. In this study, we also focused on the temporal interaction of spindles to the $\delta_I$-waves. Thus, the nesting of spindles to $\delta_I$ ($\delta_I$-Nesting; Figure 3D) was identified in a manner analogous to the “SO-Nesting” value, i.e., time differences between the spindle peak time and the time of the $\delta_I$ up-state. To quantitatively assess the changes in the temporal coupling of spindles to SO, we specifically measured as the following; time lag of spindle from the closest SO ($\Delta T_{SO\text{-}Spindle}$) was measured for each spindle event and the rate of spindles of which $\Delta T_{SO\text{-}Spindle}$ was within the nesting time window was measured; i.e., the number of SO-nested spindles / the total number of spindles × 100 % (Figures 1G and H). We also measured $\delta_I$-Nesting the same way as the “SO-Nesting” but using time lags between the peaks of spindles and the up-states of the linked $\delta_I$; i.e., the number of $\delta_I$-nested spindles / the total number of spindles × 100 % (Figures 3E and F).

**Spike activity during sleep waves—**We initially used an online sorting program (SpikePac, TDT). We then conducted offline sorting using Plexon Inc’s Offline Sorter. Only clearly identifiable units with good waveforms and a high signal-to-noise ratio were used. To assess spike activity modulation during sleep oscillations, we analyzed peri-event time histogram (PETH) and unit modulation-depth (MD). After spikes were time-locked to event reference times (e.g., SO up-states or SO-nested spindles), the PETH (bin length 20 ms) was estimated. Then, the unit MD was calculated by comparing the difference between maximum and minimum of the PETH around events time (SO-MD: within −0.5 to 0.3 sec

from SO up-states; spindles-MD: −0.25 to 0.15 sec from spindles peaks) over the baseline firing activity (averaged activity within −2 to −0.5 sec from the events for both SO-MD and spindles-MD); i.e., (maximum-minimum)/baseline firing rate. In other words, the MD is a measure of the modulation of firing rate relative to the pre-event start baseline rate. This was compared for the early period and the late period of recovery in Figure 1I and for the sham and drug conditions in Figures 4C and D. No significant change in population spike rates was found from the early to the late period (Figure S4A).

**Quantification and statistical analyses—**Figures show mean ± s.e.m.; if this was not the case, we specifically indicated it. Parametric statistics were generally used in this study (linear mixed-effect model (LME), *t*-tests, linear regression, Pearson's correlation otherwise stated); they were implemented within MATLAB. A "hierarchical nested statistics approach" of LME (using the MATLAB function "fitlme") was used for the comparison of task performance, temporal coupling of spindles, unit MD, and linear relationship (Aarts et al., 2014; Guo et al., 2021; Khanna et al., 2021; Kim et al., 2019). This was done to account for the repeated measures per animals; thus, this statistical approach ensured that the group level statistc accounted for sessions per animal and did not treat them as statistically independent samples. We fit random effects (e.g., rats) specified as an intercept for each group and reported fixed effects representing population parameters to compare (e.g., early vs late period). Adding random effects to a model recognizes correlations within sample subgroups (e.g., rat) and extends the reliability of inferences beyond the variability across multiple rats. The fixed effects were tested for P values of the linear regression slope coefficients associated with two comparing conditions. In this way, the LME accounts for the fact that units, sessions, events, or experimental conditions from the same animal are more correlated than those from different animals and is more stringent than computing statistical significance over all units, sessions, events, and conditions. The LME was used to compare $\text{stroke}_{\text{exp}}$ versus healthy conditions, early period versus late period, sham versus drug, and sleep versus no-sleep. The used random effects and fixed effects parameters are following; Figures 1H, 1I, 2B, and 3F, and Figures S2, S3, S4, and S5, random: rat, fixed: recovery period; Figure 2D, random: rat, fixed: sleep type; Figures 4B and C, random: rat, fixed: injection type. In these figures, the mean in each experiment session was used as the response parameter and two categories of the comparing conditions were used as the predictor parameter.

The LEM was also used to evaluate linear relationships or correlations between the changes in SO-Nesting and the next-day task performance in Figure 2C, between the post-training sleep duration and the within-session changes of task performance in Figure 2E, between the mean rate of $\delta_I$ preceding SO and the SO-Nesting in Figure 3H, between the mean rate of $\delta_I$ preceding SO and the next-day task performance in Figure 3I, and between the changes of SO-Nesting and the changes in spindles-MD in Figure 4D. We also used traditional linear regression or correlation to evaluate the relationship between the recovery period and the sleep metrics (e.g. SO-Nesting and $\delta_I$-Nesting) in Figures 1G and 3E, and Figure S3 left. For the comparison between distributions, we used Kolmogorov-Smirnov's test in Figure 3C and Figure S6 to test the samples were drawn from the same distribution and Bartlett's test

in Figure 1F to test equal variances (sharpness of distribution) between early period and late period.

## Supplementary Material

Refer to Web version on PubMed Central for supplementary material.

## Acknowledgements.

Research was supported by awards from the Department of Veterans Affairs, Veterans Health Administration (VA Merit: 1I01RX001640 to K.G.; VA CDA to DR, 7IK2BX003308); the Weill Neurohub, the National Institute of Neurological Disorders and Stroke (5K02NS093014 to K.G.; K99NS119737 to J.K.); American Heart Association Postdoctoral Fellowship (831442 to J.K.); and the Basic Science Research Program through the National Research Foundation of Korea (2018R1A6A3A03013031 to J.K.). Karunesh Ganguly, M.D., Ph.D., and Dhakshin Ramanathan, MD., PhD hold a Career Award for Medical Scientists from the Burroughs Wellcome Fund.

## REFERENCES

Aarts E, Verhage M, Veenvliet JV, Dolan CV, and van der Sluis S (2014). A solution to dependency: using multilevel analysis to accommodate nested data. Nature neuroscience 17, 491–496. [PubMed: 24671065]

Antony JW, Piloto L, Wang M, Pacheco P, Norman KA, and Paller KA (2018). Sleep Spindle Refractoriness Segregates Periods of Memory Reactivation. Curr Biol 28, 1736–1743 e1734. [PubMed: 29804809]

Backhaus W, Braass H, Gerloff C, and Hummel FC (2018). Can Daytime Napping Assist the Process of Skills Acquisition After Stroke? Frontiers in neurology 9, 1002. [PubMed: 30524365]

Baumann CR, Kilic E, Petit B, Werth E, Hermann DM, Tafti M, and Bassetti CL (2006). Sleep EEG changes after middle cerebral artery infarcts in mice: different effects of striatal and cortical lesions. Sleep 29, 1339–1344. [PubMed: 17068988]

Bergmann TO, and Born J (2018). Phase-Amplitude Coupling: A General Mechanism for Memory Processing and Synaptic Plasticity? Neuron 97, 10–13. [PubMed: 29301097]

Bernardi G, Siclari F, Handjaras G, Riedner BA, and Tononi G (2018). Local and Widespread Slow Waves in Stable NREM Sleep: Evidence for Distinct Regulation Mechanisms. Front Hum Neurosci 12, 248. [PubMed: 29970995]

Bernhardt J, Hayward KS, Kwakkel G, Ward NS, Wolf SL, Borschmann K, Krakauer JW, Boyd LA, Carmichael ST, and Corbett D (2017). Agreed definitions and a shared vision for new standards in stroke recovery research: the stroke recovery and rehabilitation roundtable taskforce. International Journal of Stroke 12, 444–450. [PubMed: 28697708]

Born J, Rasch B, and Gais S (2006). Sleep to remember. Neuroscientist 12, 410–424. [PubMed: 16957003]

Burns BD (1951). Some properties of isolated cerebral cortex in the unanaesthetized cat. The Journal of physiology 112, 156. [PubMed: 14825189]

Burns BD, and Webb AC (1979). The correlation between discharge times of neighbouring neurons in isolated cerebral cortex. Proceedings of the Royal Society of London Series B Biological Sciences 203, 347–360. [PubMed: 34158]

Buzsáki G (2015). Hippocampal sharp wave-ripple: A cognitive biomarker for episodic memory and planning. Hippocampus 25, 1073–1188. [PubMed: 26135716]

Cairney SA, Guttesen AAV, El Marj N, and Staresina BP (2018). Memory Consolidation Is Linked to Spindle-Mediated Information Processing during Sleep. Curr Biol 28, 948–954 e944. [PubMed: 29526594]

Carmichael ST, and Chesselet MF (2002). Synchronous neuronal activity is a signal for axonal sprouting after cortical lesions in the adult. Journal of Neuroscience 22, 6062–6070. [PubMed: 12122067]

Clarkson AN, Huang BS, Macisaac SE, Mody I, and Carmichael ST (2010). Reducing excessive GABA-mediated tonic inhibition promotes functional recovery after stroke. Nature 468, 305–309. [PubMed: 21048709]

de Vivo L, Bellesi M, Marshall W, Bushong EA, Ellisman MH, Tononi G, and Cirelli C (2017). Ultrastructural evidence for synaptic scaling across the wake/sleep cycle. Science 355, 507–510. [PubMed: 28154076]

Dromerick AW, Geed S, Barth J, Brady K, Giannetti ML, Mitchell A, Edwardson MA, Tan MT, Zhou Y, Newport EL, et al. (2021). Critical Period After Stroke Study (CPASS): A phase II clinical trial testing an optimal time for motor recovery after stroke in humans. Proceedings of the National Academy of Sciences of the United States of America 118.

Dromerick AW, Lang CE, Birkenmeier RL, Wagner JM, Miller JP, Videen TO, Powers WJ, Wolf SL, and Edwards DF (2009). Very Early Constraint-Induced Movement during Stroke Rehabilitation (VECTORS) A single-center RCT. Neurology 73, 195–201. [PubMed: 19458319]

Duss SB, Seiler A, Schmidt MH, Pace M, Adamantidis A, Muri RM, and Bassetti CL (2017). The role of sleep in recovery following ischemic stroke: A review of human and animal data. Neurobiol Sleep Circadian Rhythms 2, 94–105. [PubMed: 31236498]

Egert D PJ, Batmutsky I, Caldwell CM, Roossien J, Patel PR, Lemke S, Ganguly K, Cai D, Chestek CA, Berke JD (2018). Cellular-scale probes for high-density, precisely-localized neurophysiology. Paper presented at: Society for Neuroscience Annual Meeting: available at https://wwwabstractsonlinecom/pp8/#!/4649/presentation/24873.

Facchin L, Schone C, Mensen A, Bandarabadi M, Pilotto F, Saxena S, Libourel PA, Bassetti CLA, and Adamantidis AR (2020). Slow Waves Promote Sleep-Dependent Plasticity and Functional Recovery after Stroke. The Journal of neuroscience : the official journal of the Society for Neuroscience 40, 8637–8651. [PubMed: 33087472]

Ganguly K, Byl NN, and Abrams GM (2013). Neurorehabilitation: Motor Recovery After Stroke as an Example. Annals of Neurology 74, 373–381. [PubMed: 25813243]

Gao B, Cam E, Jaeger H, Zunzunegui C, Sarnthein J, and Bassetti CL (2010). Sleep disruption aggravates focal cerebral ischemia in the rat. Sleep 33, 879–887. [PubMed: 20614848]

Genzel L, Kroes MC, Dresler M, and Battaglia FP (2014). Light sleep versus slow wave sleep in memory consolidation: a question of global versus local processes? Trends in neurosciences 37, 10–19. [PubMed: 24210928]

Giubilei F, Iannilli M, Vitale A, Pierallini A, Sacchetti M, Antonini G, and Fieschi C (1992). Sleep patterns in acute ischemic stroke. Acta neurologica scandinavica 86, 567–571. [PubMed: 1481642]

Gottselig JM, Bassetti CL, and Achermann P (2002). Power and coherence of sleep spindle frequency activity following hemispheric stroke. Brain : a journal of neurology 125, 373–383. [PubMed: 11844737]

Gulati T, Guo L, Ramanathan DS, Bodepudi A, and Ganguly K (2017). Neural reactivations during sleep determine network credit assignment. Nature neuroscience 20, 1277–1284. [PubMed: 28692062]

Gulati T, Ramanathan DS, Wong CC, and Ganguly K (2014). Reactivation of emergent task-related ensembles during slow-wave sleep after neuroprosthetic learning. Nature neuroscience 17, 1107–1113. [PubMed: 24997761]

Gulati T, Won SJ, Ramanathan DS, Wong CC, Bodepudi A, Swanson RA, and Ganguly K (2015). Robust neuroprosthetic control from the stroke perilesional cortex. The Journal of neuroscience : the official journal of the Society for Neuroscience 35, 8653–8661. [PubMed: 26041930]

Guo L, Kondapavulur S, Lemke SM, Won SJ, and Ganguly K (2021). Coordinated increase of reliable cortical and striatal ensemble activations during recovery after stroke. Cell Rep 36, 109370. [PubMed: 34260929]

He WM, Ying-Fu L, Wang H, and Peng YP (2019). Delayed treatment of alpha5 GABAA receptor inverse agonist improves functional recovery by enhancing neurogenesis after cerebral ischemia-reperfusion injury in rat MCAO model. Sci Rep 9, 2287. [PubMed: 30783142]

Helfrich RF, Mander BA, Jagust WJ, Knight RT, and Walker MP (2018). Old Brains Come Uncoupled in Sleep: Slow Wave-Spindle Synchrony, Brain Atrophy, and Forgetting. Neuron 97, 221–230. [PubMed: 29249289]

Ito HT, Zhang SJ, Witter MP, Moser EI, and Moser MB (2015). A prefrontal-thalamo-hippocampal circuit for goal-directed spatial navigation. Nature 522, 50–55. [PubMed: 26017312]

Khanna P, Totten D, Novik L, Roberts J, Morecraft RJ, and Ganguly K (2021). Low-frequency stimulation enhances ensemble co-firing and dexterity after stroke. Cell 184, 912–930 e920. [PubMed: 33571430]

Kim J, Gulati T, and Ganguly K (2019). Competing Roles of Slow Oscillations and Delta Waves in Memory Consolidation versus Forgetting. Cell 179, 514–526 e513. [PubMed: 31585085]

Kim JK, and Fiorillo CD (2017). Theory of optimal balance predicts and explains the amplitude and decay time of synaptic inhibition. Nat Commun 8, 14566. [PubMed: 28281523]

Klinzing JG, Niethard N, and Born J (2019). Mechanisms of systems memory consolidation during sleep. Nature neuroscience 22, 1598–1610. [PubMed: 31451802]

Korman M, Doyon J, Doljansky J, Carrier J, Dagan Y, and Karni A (2007). Daytime sleep condenses the time course of motor memory consolidation. Nature neuroscience 10, 1206–1213. [PubMed: 17694051]

Krakauer JW, Carmichael ST, Corbett D, and Wittenberg GF (2012). Getting neurorehabilitation right: what can be learned from animal models? Neurorehabilitation and neural repair 26, 923–931. [PubMed: 22466792]

Latchoumane CFV, Ngo HVV, Born J, and Shin HS (2017). Thalamic Spindles Promote Memory Formation during Sleep through Triple Phase-Locking of Cortical, Thalamic, and Hippocampal Rhythms. Neuron 95, 424–435. [PubMed: 28689981]

Lemke SM, Ramanathan DS, Darevksy D, Egert D, Berke JD, and Ganguly K (2021). Coupling between motor cortex and striatum increases during sleep over long-term skill learning. Elife 10, e64303. [PubMed: 34505576]

Levy RM, Harvey RL, Kissela BM, Winstein CJ, Lutsep HL, Parrish TB, Cramer SC, and Venkatesan L (2016). Epidural Electrical Stimulation for Stroke Rehabilitation: Results of the Prospective, Multicenter, Randomized, Single-Blinded Everest Trial. Neurorehabil Neural Repair 30, 107–119. [PubMed: 25748452]

Macdonell RA, Donnan GA, Bladin PF, Berkovic SF, and Wriedt CH (1988). The electroencephalogram and acute ischemic stroke. Distinguishing cortical from lacunar infarction. Archives of neurology 45, 520–524. [PubMed: 3358704]

Maingret N, Girardeau G, Todorova R, Goutierre M, and Zugaro M (2016). Hippocampo-cortical coupling mediates memory consolidation during sleep. Nature neuroscience 19, 959–964. [PubMed: 27182818]

Marshall L, Helgadottir H, Molle M, and Born J (2006). Boosting slow oscillations during sleep potentiates memory. Nature 444, 610–613. [PubMed: 17086200]

Molle M, Yeshenko O, Marshall L, Sara SJ, and Born J (2006). Hippocampal sharp wave-ripples linked to slow oscillations in rat slow-wave sleep. Journal of neurophysiology 96, 62–70. [PubMed: 16611848]

Ngo H-VV, Miedema A, Faude I, Martinetz T, Mölle M, and Born J (2015). Driving sleep slow oscillations by auditory closed-loop stimulation—a self-limiting process. Journal of Neuroscience 35, 6630–6638. [PubMed: 25926443]

Ngo HV, Martinetz T, Born J, and Molle M (2013). Auditory closed-loop stimulation of the sleep slow oscillation enhances memory. Neuron 78, 545–553. [PubMed: 23583623]

Nita DA, Cisse Y, Timofeev I, and Steriade M (2007). Waking-sleep modulation of paroxysmal activities induced by partial cortical deafferentation. Cereb Cortex 17, 272–283. [PubMed: 16495431]

Norrving B, and Kissela B (2013). The global burden of stroke and need for a continuum of care. Neurology 80, S5–12. [PubMed: 23319486]

Pack AI, Galante RJ, Maislin G, Cater J, Metaxas D, Lu S, Zhang L, Von Smith R, Kay T, Lian J, et al. (2007). Novel method for high-throughput phenotyping of sleep in mice. Physiol Genomics 28, 232–238. [PubMed: 16985007]

Pearson-Fuhrhop KM, Kleim JA, and Cramer SC (2009). Brain plasticity and genetic factors. Top Stroke Rehabil 16, 282–299. [PubMed: 19740733]

Peyrache A, Khamassi M, Benchenane K, Wiener SI, and Battaglia FP (2009). Replay of rule-learning related neural patterns in the prefrontal cortex during sleep. Nature neuroscience 12, 919–926. [PubMed: 19483687]

Poryazova R, Huber R, Khatami R, Werth E, Brugger P, Barath K, Baumann CR, and Bassetti CL (2015). Topographic sleep EEG changes in the acute and chronic stage of hemispheric stroke. Journal of sleep research 24, 54–65. [PubMed: 25159577]

Ramanathan DS, Gulati T, and Ganguly K (2015). Sleep-Dependent Reactivation of Ensembles in Motor Cortex Promotes Skill Consolidation. PLoS Biol 13, e1002263. [PubMed: 26382320]

Ramanathan DS, Guo L, Gulati T, Davidson G, Hishinuma AK, Won SJ, Knight RT, Chang EF, Swanson RA, and Ganguly K (2018). Low-frequency cortical activity is a neuromodulatory target that tracks recovery after stroke. Nature Medicine 24, 1257-+.

Robinson MJ, Macrae IM, Todd M, Reid JL, and McCulloch J (1990). Reduction of local cerebral blood flow to pathological levels by endothelin-1 applied to the middle cerebral artery in the rat. Neurosci Lett 118, 269–272. [PubMed: 2274283]

Roome RB, Bartlett RF, Jeffers M, Xiong J, Corbett D, and Vanderluit JL (2014). A reproducible Endothelin-1 model of forelimb motor cortex stroke in the mouse. J Neurosci Methods 233, 34–44. [PubMed: 24915635]

Rothschild G, Eban E, and Frank LM (2017). A cortical-hippocampal-cortical loop of information processing during memory consolidation. Nature neuroscience 20, 251–259. [PubMed: 27941790]

Sarasso S, D'Ambrosio S, Fecchio M, Casarotto S, Vigano A, Landi C, Mattavelli G, Gosseries O, Quarenghi M, Laureys S, et al. (2020). Local sleep-like cortical reactivity in the awake brain after focal injury. Brain : a journal of neurology.

Sharkey J, Ritchie IM, and Kelly PA (1993). Perivascular microapplication of endothelin-1: a new model of focal cerebral ischaemia in the rat. J Cereb Blood Flow Metab 13, 865–871. [PubMed: 8360292]

Siengsukon CF, and Boyd LA (2009). Sleep to learn after stroke: implicit and explicit off-line motor learning. Neurosci Lett 451, 1–5. [PubMed: 19121365]

Silversmith DB, Lemke SM, Egert D, Berke JD, and Ganguly K (2020). The Degree of Nesting between Spindles and Slow Oscillations Modulates Neural Synchrony. Journal of Neuroscience 40, 4673–4684. [PubMed: 32371605]

Sirota A, Csicsvari J, Buhl D, and Buzsaki G (2003). Communication between neocortex and hippocampus during sleep in rodents. Proceedings of the National Academy of Sciences of the United States of America 100, 2065–2069. [PubMed: 12576550]

Staresina BP, Bergmann TO, Bonnefond M, van der Meij R, Jensen O, Deuker L, Elger CE, Axmacher N, and Fell J (2015). Hierarchical nesting of slow oscillations, spindles and ripples in the human hippocampus during sleep. Nature neuroscience 18, 1679–1686. [PubMed: 26389842]

Stickgold R (2005). Sleep-dependent memory consolidation. Nature 437, 1272–1278. [PubMed: 16251952]

Tononi G, and Cirelli C (2014). Sleep and the price of plasticity: from synaptic and cellular homeostasis to memory consolidation and integration. Neuron 81, 12–34. [PubMed: 24411729]

Topolnik L, Steriade M, and Timofeev I (2003). Partial cortical deafferentation promotes development of paroxysmal activity. Cereb Cortex 13, 883–893. [PubMed: 12853375]

Tu-Chan AP, Natraj N, Godlove J, Abrams G, and Ganguly K (2017). Effects of somatosensory electrical stimulation on motor function and cortical oscillations. J Neuroeng Rehabil 14, 113. [PubMed: 29132379]

van Dellen E, Hillebrand A, Douw L, Heimans JJ, Reijneveld JC, and Stam CJ (2013). Local polymorphic delta activity in cortical lesions causes global decreases in functional connectivity. Neuroimage 83, 524–532. [PubMed: 23769919]

Virley D, Hadingham SJ, Roberts JC, Farnfield B, Elliott H, Whelan G, Golder J, David C, Parsons AA, and Hunter AJ (2004). A new primate model of focal stroke: endothelin-1-induced middle cerebral artery occlusion and reperfusion in the common marmoset. J Cereb Blood Flow Metab 24, 24–41. [PubMed: 14688614]

Walker MP, Brakefield T, Morgan A, Hobson JA, and Stickgold R (2002). Practice with sleep makes perfect: sleep-dependent motor skill learning. Neuron 35, 205–211. [PubMed: 12123620]

Whishaw IQ, Oconnor WT, and Dunnett SB (1986). The Contributions of Motor Cortex, Nigrostriatal Dopamine and Caudate-Putamen to Skilled Forelimb Use in the Rat. Brain : a journal of neurology 109, 805–843. [PubMed: 3779371]

Wong CC, Ramanathan DS, Gulati T, Won SJ, and Ganguly K (2015). An automated behavioral box to assess forelimb function in rats. J Neurosci Methods 246, 30–37. [PubMed: 25769277]

Xia F, Richards BA, Tran MM, Josselyn SA, Takehara-Nishiuchi K, and Frankland PW (2017). Parvalbumin-positive interneurons mediate neocortical-hippocampal interactions that are necessary for memory consolidation. Elife 6, e27868. [PubMed: 28960176]

Yang G, Lai CS, Cichon J, Ma L, Li W, and Gan WB (2014). Sleep promotes branch-specific formation of dendritic spines after learning. Science 344, 1173–1178. [PubMed: 24904169]

Yizhar O, Fenno LE, Prigge M, Schneider F, Davidson TJ, O'Shea DJ, Sohal VS, Goshen I, Finkelstein J, Paz JT, et al. (2011). Neocortical excitation/inhibition balance in information processing and social dysfunction. Nature 477, 171–178. [PubMed: 21796121]

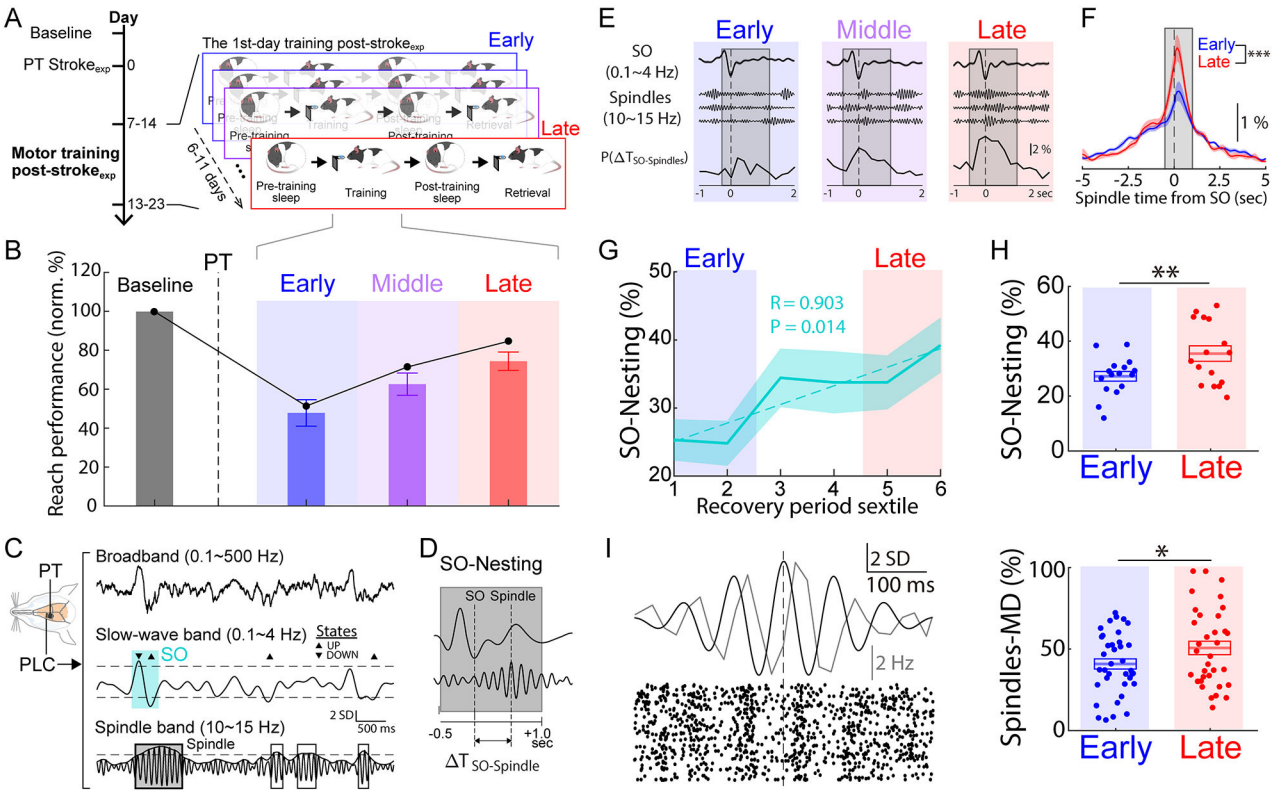


**Figure 1. Reach performance and redistribution of spindles toward SO over recovery.**

**(A)**, Experimental flow. PT=photothrombotic stroke$_{exp}$.

**(B)**, Mean retrieval success rates (n=8 rats; black dots: two-session average per period for single animal). Bars show average of sessions in tertiles.

**(C)**, Examples of broadband (0.1-500 Hz) and filtered (0.1-4 Hz SO; 10-15 Hz spindles) trace in PLC. SO=cyan and spindle=gray. Open boxes show non-spindle events.

**(D)**, Cartoons of SO-Nesting. Nesting window −0.5-1.0 sec from SO up-state; same as 'E' and 'F').

**(E)**, Examples of SO-spindle interaction. Mean SO-up-state-triggered LFP. Three single-trial examples of detected spindles near SO (middle). Examples of probability distribution (bottom).

**(F)**, Comparison in distributions of $\Delta T_{SO\text{-}Spindles}$ between early and late (n = 16 sessions, 8 rats; Bartlett's test, $X^2 = 58.7$, ***$P < 10^{-13}$).

**(G)**, Average time courses of SO-Nesting and $\delta_I$-Nesting over recovery (n = 8 rats). Dashed is linear regression (R = 0.903, P = 0.014).

**(H)**, SO-Nesting early vs. late (early, n = 16 sessions in 8 rats, 27.2 ± 1.7% vs. late, n = 16 sessions in 8 rats, 35.5 ± 2.8%, LME, $t_{30} = 3.58$, **P = 0.011; using averages per period, early, n = 8 rats, 27.2 ± 2.4% vs. late, n = 8 rats, 35.5 ± 3.5%, LME, $t_{14} = 3.58$, **P = 3.0 x $10^{-3}$).

**(I)**, Left, average of event-triggered LFP (10~15 Hz; black), spike rates (gray), and raster plot of an example unit. Right, unit modulation depth (MD) during spindles for early (n = 37 units, 8 rats; 40.9 ± 3.1%) and late (n = 34 units, 8 rats; 50.7 ± 4.1%). There were significant changes from early to late (LME, $t_{69} = 2.21$, *P = 0.030).

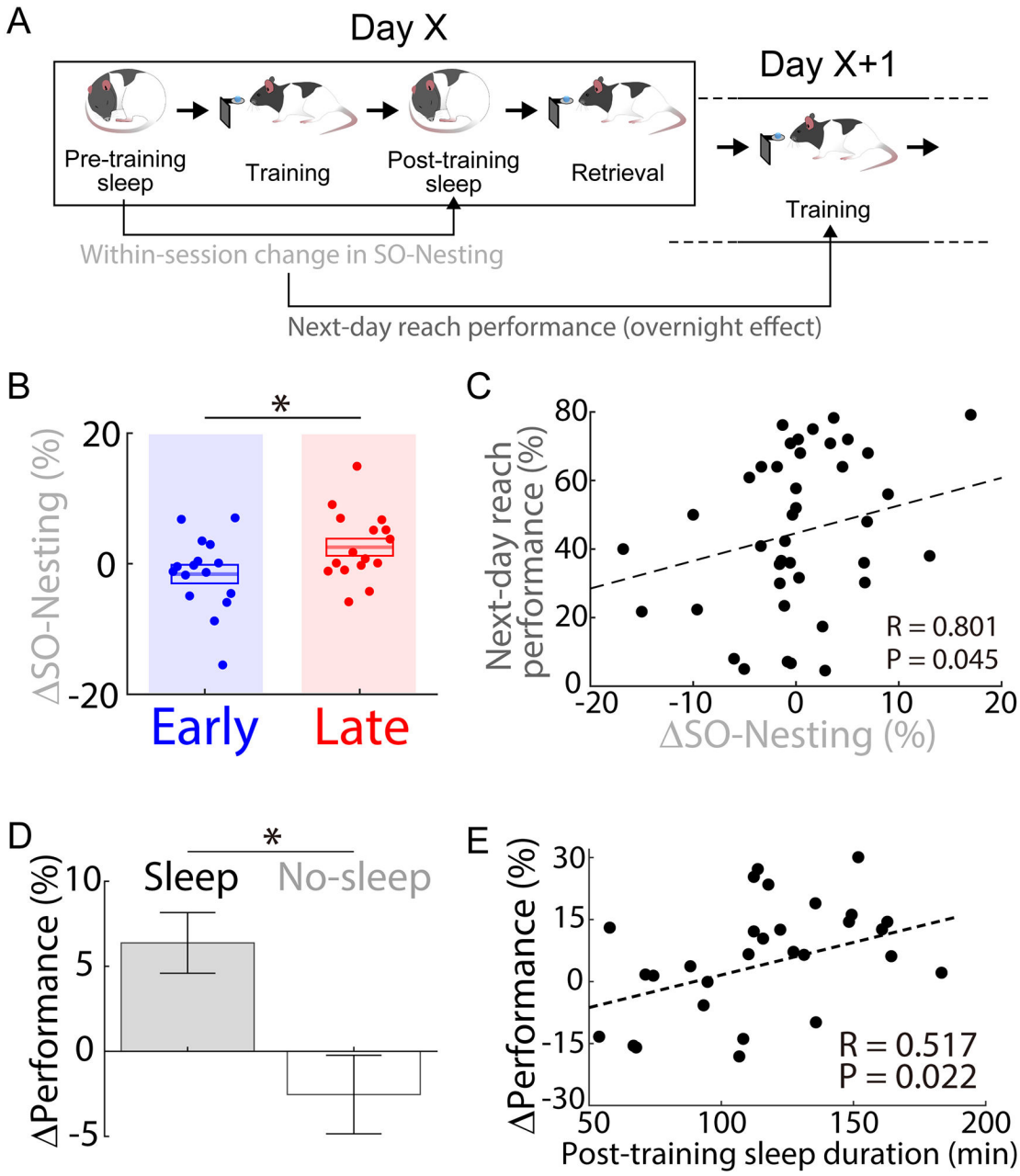


**Figure 2. Spindle redistribution and offline gains.**

**(A)**, Within-session changes (i.e., changes in Day X) of SO-Nesting compared with next-day (Day X+1) performance.

**(B)**, Comparison of changes in the SO-Nesting within a session (ΔSO-Nesting: early, n = 16 sessions in 8 rats, −1.6 ± 1.4% vs. late, n = 16 sessions in 8 rats, 2.6 ± 1.3%, LME, $t_{30}$ = 2.24, *P = 0.032).

**(C)**, Relationship of ΔSO-Nesting to the next-day performance over recovery (LME fit, R = 0.801, P = 0.045; n = 40 sessions in 8 rats, 5 pairs per animal).

**(D)**, Within-session changes in the motor performance (ΔPerformance; changes from reach training to retrieval) during the recovery $_{p}$ (sleep, n = 29 sessions in 6 rats: 6.4 ± 1.8%;

no-sleep, n = 28 sessions in 8 rats: −2.5 ± 2.3%; sleep vs. no-sleep, LME, $t_{55} = -2.31$, *P = 0.024).

**(E)**, Relationship of post-training sleep duration to changes in performance (LME fit, R = 0.517, P = 0.022).

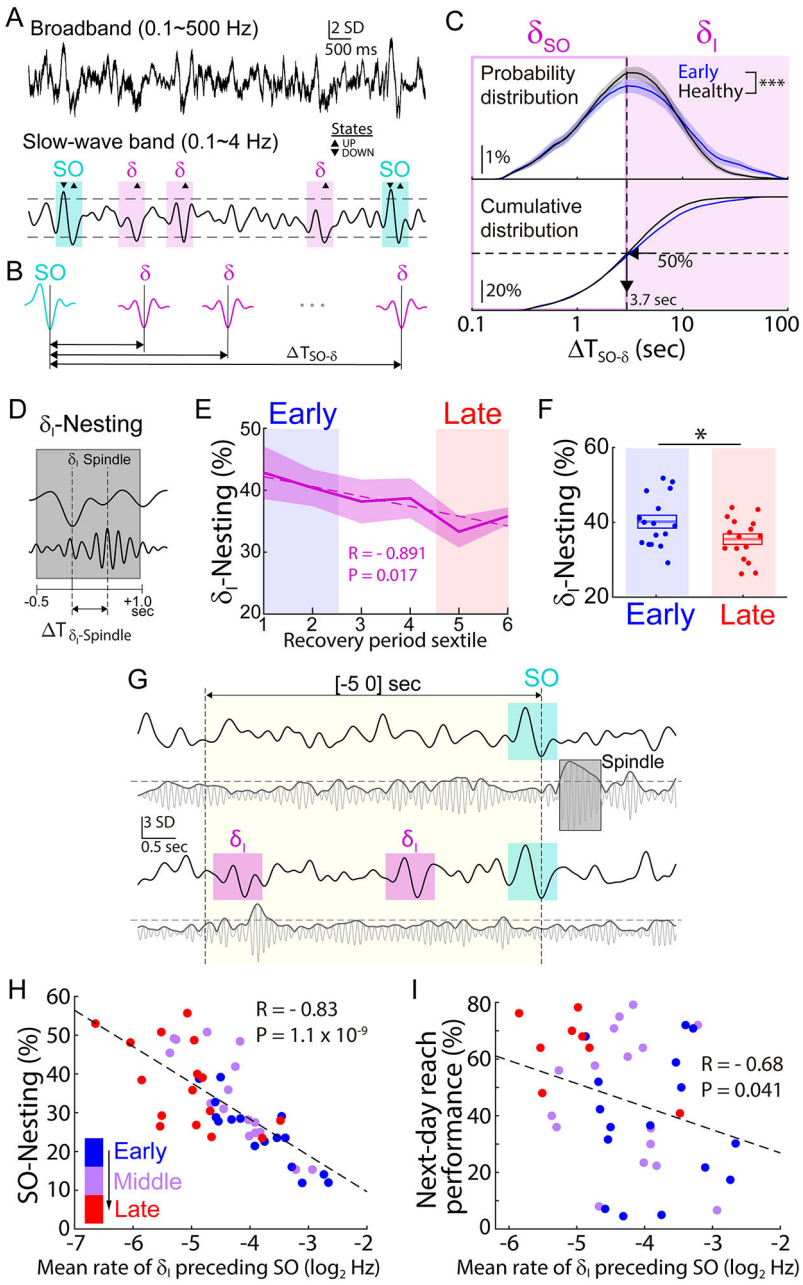


**Figure 3. Pathological increase of $\delta_I$.**

**(A)**, Examples of broadband (0.1-500 Hz) and filtered (0.1-4 Hz).

**(B)**, Schematic showing the temporal distance of δ-waves from SO ($\Delta T_{SO-\delta}$).

**(C)**, Comparison of SO-coupled δ ($\delta_{SO}$) and isolated δ ($\delta_I$) for early stroke (blue; n = 16 sessions, 8 rats) and healthy (black; n = 9 sessions, 5 rats; Kolmogorov-Smirnov test, KS-statistic = 0.17, ***$P < 10^{-15}$). Average distributions of $\Delta T_{SO-\delta}$ are shown. $\delta_{SO}$ and $\delta_I$ waves were separated by the 50th percentile (3.7 sec, vertical dashed line) from the distribution of healthy.

**(D)**, Cartoon of nesting of spindle to $\delta_I$ ($\delta_I$-Nesting).

**(E)**, $\delta_I$-Nesting over recovery (n = 8 rats). Dashed is linear regression (R = −0.891, P = 0.017).

**(F)**, Comparison of $\delta_I$-Nesting between early vs. late (early, n = 16 sessions in 8 rats, 40.1 ± 1.7% vs. late, n = 16 sessions in 8 rats, 35.4 ± 1.4%, LME, $t_{30}$ = −2.27, *P = 0.031; using average per period, early, n = 8 rats, 40.1 ± 2.3% vs. late, n = 8 rats, 35.4 ± 1.7%, LME, $t_{14}$ = −1.74, **P = 0.10).

**(G)**, Top, LFP traces filtered at slow-wave band and spindle band (case where no $\delta_I$-wave preceded SO during −5-0s from a SO up-state (yellow box). Bottom, same a case where two $\delta_I$-waves preceded SO −5-0s from a SO up-state.

**(H)**, Relationship between the mean rate of $\delta_I$-waves preceding SO within 5 sec and the SO-Nesting over all recovery sextiles. There was a negative correlation (n = 48 sessions in 8 rats, 6 pairs per animal; dashed line, LME fit, R = −0.83, P = 1.1 x $10^{-9}$).

**(I)**, Relationship between the mean rate of $\delta_I$-waves preceding SO within 5 sec to the next-day reach performance. There was a negative correlation (n = 40 sessions in 8 rats, 5 pairs per animal; LME fit, R = −0.68, P = 0.041).

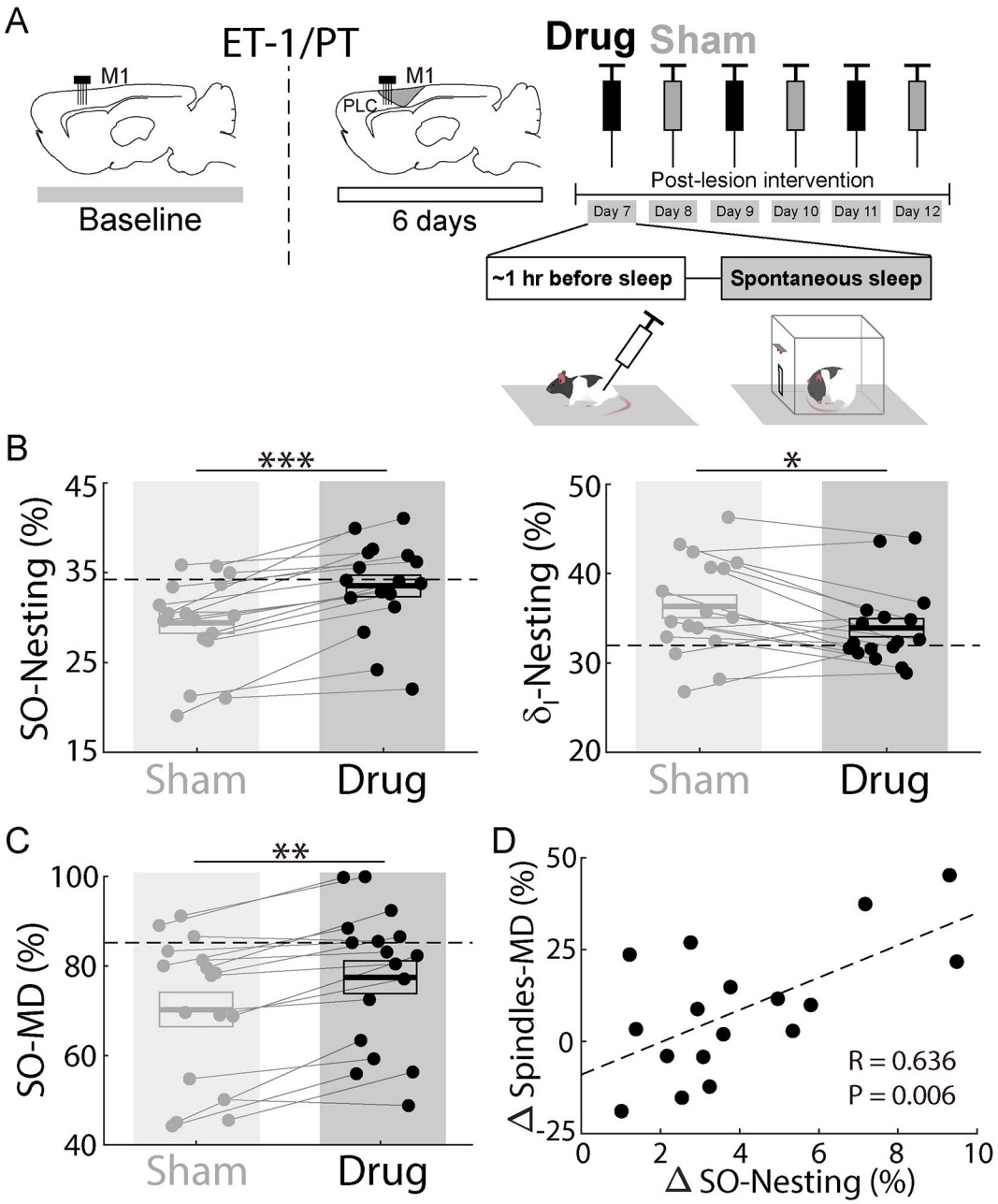


**Figure 4. Blocking $GABA_A$ α5-subtype receptor increases SO-Nesting.**

**(A)**, LFP/spike was monitored in PLC (n = 6 rats). Either ET-1 (n = 3) or PT (n = 3) was induced. In ET-1, LFP/spike activity was recorded 2~3 days before inducing $stroke_{exp}$ (vertical dashed line) for baseline. Either L655-708 (drug) or saline (sham) was administrated IP on separate days.

**(B)**, Comparison of SO-Nesting and $\delta_I$-Nesting. SO-Nesting and $\delta_I$-Nesting was stronger and weaker, respectively, with drug compared to sham (SO-Nesting: sham, n = 17 sessions, 29.4 ± 1.2% vs. drug, n = 17 sessions, 33.5 ± 1.2%, LME, $t_{32} = 6.93$, ***$P < 10^{-7}$; $\delta_I$-Nesting: sham, 36.3 ± 1.3% vs. drug, 33.9 ± 1.0%, LME, $t_{32} = -2.29$, *P = 0.028). Baseline in horizontal dashed line.

**(C)**, Comparison of unit MD during SO (SO-MD: sham, 70.3 ± 3.8% vs. drug, 77.5 ± 3.7%, LME, $t_{32} = 2.79$, **P < 0.01).

**(D)**, Relationship of change of SO-Nesting in 'B' to MD during spindles. There was a positively significant correlation (LME fit, R = 0.636, P = 0.006).

## KEY RESOURCES TABLE

| REAGENT or RESOURCE | SOURCE | IDENTIFIER |
|---|---|---|
| Chemicals, Peptides, and Recombinant Proteins | | |
| Rose bengal | Sigma-Aldrich | CAS# 330000 |
| Endothelin-1 | Sigma-Aldrich | CAS# 117399-94-7 |
| L655,708 | Sigma-Aldrich | CAS# 130477-52-0 |
| Experimental Models: Organisms/Strains | | |
| Long Evans Rat | Charles River Labs | Strain Code 006 |
| Software and Algorithms | | |
| Offline Sorter v4.6.0 | Plexon Inc | https://plexon.com/products/offline-sorter |
| SpikePac | Tucker-Davis Technologies (TDT) | https://www.tdt.com/support/downloads/ |
| MATLAB R2020a | Mathworks | https://www.mathworks.com/products/matlab.html |
| SO, δ-waves, and spindles detection algorithms | Zenodo | DOI: 10.5281/zenodo.5911914 |
| Other | | |
| 32-channel microwire electrode arrays | Tucker-Davis Technologies (TDT) | https://www.tdt.com/component/zif-clip-array-electrodes/ |
| 32-channel microwire electrode arrays | Innovative Neurophysiology Inc | http://www.inphysiology.com/optogenetic-applications/ |
| 128-channel custom electrode arrays | Egert et al., 2018 | https://wwwabstractsonlinecom/pp8/#!/4649/presentation/24873 |
| RHD 128-Channel recording headstage | Intan Technologies | https://intantech.com/RHD_headstages.html?tabSelect=RHD128ch |
| Infusion cannula | P1 Technologies | Cat# C315GS<br>Cat# C235G |